Journal of Applied Fluid Mechanics, Vol. 18, No. 3, pp. 549-566, 2025.
Available online at www.jafmonline.net, ISSN 1735-3572, EISSN 1735-3645.
https://doi.org/10.47176/jafm.18.3.2843

Numerical Investigation of Clocking Effect on Fluctuating Characters and Radial Force within Impeller for a Centrifugal Pump

X. Zhu [1], X. Han [1], C. Xie [2], H. Zhang [1,3†] and W. Jiang [4]

[1] *Shandong Jianzhu University, Jinan 250101, China*
[2] *Shanghai Marine Equipment Research Institute, Shanghai 200030, China*
[3] *University of Birmingham, Edgbaston, Birmingham B15 2TT UK*
[4] *Northwest A&F University; Yangling 712100, China*

†*Corresponding Author Email: qdzhanghao@126.com*

ABSTRACT

The present work aims to investigate the influence of vane clocking effect on fluctuating characters and radial force on impeller for centrifugal pump. Numerical simulations were conducted with validation by experiments, at four different relative angular position between vane and tongue. The power consumption and work done by blades are evaluated in time-history. The radial velocity, circumferential velocity at impeller-diffuser clearance is depicted by expanding the turning surface, for comparison under different diffuser position to reveal the flow distortion affected by clocking effect. The results indicate that when vane trailing edge is at tongue (θ_{d1}), the corresponding diffuser channel is placed against small flow section in volute leading to a blocking effect that results in significant circumferential inhomogeneity at diffuser outlet. The interaction between impeller blade and different diffuser vane presents distinct intensity, causing the unsteady fluctuation intensity of power consumption of impeller at different vane positions is significantly different, and so is the radial force. As the diffuser vane moves away from tongue (at θ_{d4}), the blocking effect reduces and the flow field becomes more evenly distributed among each channel. Resulting in weaker fluctuations in the power consumption, blade load and radial force.

Article History

Received May 14, 2024
Revised September 2, 2024
Accepted September 21, 2024
Available online January 1, 2025

Keywords:

Clocking effect
Centrifugal pump
Vaned diffuser
Blade load
Blocking effect

1. INTRODUCTION

In turbomachinery, the clocking effect refers to the changes in mechanical performance and flow characteristics caused by the relative angular position between two stators or two rotors. This phenomenon has a significant impact on the overall performance of the turbomachinery, and first appeared in the study of turbines (Walker & Oliver, 1972). Subsequently, many scholars conducted more in-depth research on the phenomenon of clocking effect in turbomachinery (Huber et al., 1996; Dorney et al., 1998; Arnone et al., 2002). Studies on the clocking effect (Billiard et al., 2008, König et al., 2009) in turbomachinery such as turbines and compressors have shown that changes in the clocking position can significantly affect the aerodynamic characters such as load of the blades, pressure fluctuations, efficiency, and other performance parameters. Additionally, clocking effect in centrifugal pumps or pump as turbine is also proposed in research work recently (Hongyu et al., 2021; Zhang et al. 2021). The clocking effect in centrifugal pumps refers to the operating characters of the pump changes significantly with different relative angular position between rotors or stators, like vane and volute tongue, impeller and inducer, impeller and impeller in multistage pumps. The clocking effect due to inducer or inlet vanes are studied to demonstrated the change of operating parameters due to different clocking position (Qu et al., 2016; Tan et al., 2016, 2019; Yang et al., 2019).

For centrifugal pumps with vaned diffuser, different relative angular positions between the outlet vane and tongue affect the operating characters obviously. Zhang et al. (2021) investigated the influence of vane clocking effect on hydrodynamic characteristics of a single-stage centrifugal pump with a radial vaned diffuser. The study found that there is an optimum position of vanes that can increase the pump head and efficiency while reducing the intensity of pressure fluctuations. The clocking position of the radial vaned diffusers was found to significantly affect the velocity homogeneity at the impeller outlet. Gu et al. (2019) studied the variation of hydraulic performance under vane clocking effect by flow loss visualization

NOMENCLATURE

A_2	area of impeller outlet	θ_d	diffuser angular position
C_{pa}	averaged pressure	Q_{des}	design flow rate
C_{pf}	pressure coefficient at dominant frequency	W_{sft}	shaft power
C_{psdv}	standard deviation of pressure	n_S	specific speed
F	force	u_2	speed of blade trailing edge
H_{des}	design head	θ_r	angular coordinate of blade trailing edge
M	tongue	Φ	head coefficient

method. The results show that vane clocking position affect the relative head monotonic increasingly as flow rate rises. The hydraulic efficiency at design and overload flows changes obviously with clocking position varies. Guan et al. (2021) studied the clocking effect in centrifugal pump. They found that the clocking effect affect the pressure fluctuation and the unsteady radial force imposed on the impeller greatly. They suggested that to obtain better performance and improve the flow field, the volute tongue should be located near the middle of two diffuser vanes. Zhu et al. (2023) proposed detailed flow information to reveal the clocking effect on energy loss in centrifugal pump. The results show clocking effect has a significant influence on hydraulic loss in volute more than other components. Lai et al. (2020) assess the influence of clocking effect by evaluating the flow rate in impeller and diffuser passages. They found that and flow rate distribution is affected greatly by diffuser installation angles. Wang et al. (2018) studied the influence of clocking effect on the hydraulic performance and pressure fluctuation of centrifugal pump. They found that maximum efficiency difference under difference diffuser position is up to 1.5%. The position of the diffuser vanes relative to the tongue can significantly impact the flow field and result in variations in pressure distribution and pulsation. The researched of Wei et al. (2018) and Jiang et al. (2016) proposed that there exists optimized position for vane installing to obtain more improved flow field.

With the development of computational fluid dynamics (CFD) technology, CFD techniques has been widely implemented in investigations on turbomachinery for its time-saving, low-cost and convenient to conduct features, especially for its ability to depict and fully display the flow information of the entire flow field inside turbomachinery (Li et al, 2024a). Ma et al. (2017) studied dynamic characters in multiphase pump by CFD method with SST k-ω turbulence model. Gong et al. (2022) studied the correlative mechanism of the ambient pressure and inflow uniformity on the vortex and cavitation by CFD technic with k-ε turbulence model combined with mixture model.

Wang et al. (2022), Shi et al. (2021) and Rogovyi et al. (2021) conducted numerical studies on pumps with SST k-ω turbulence model to study variation of the unsteady flow field. Besides different turbulence models like LES model (Han et al., 2020; Posa, 2021), sas-sst turbulence model (Xiaoran et al. 2018; Ennouri et al., 2019; Li et al, 2024b) is adopted to study the unsteady characters such as pressure pulsation, velocity fluctuation and energy loss in centrifugal pumps.

Since centrifugal pumps operate in a rotating frame with strict symmetric rotating impellers and static diffusers, the relative angular position between the outlet vane and tongue forms different physical boundary downstream of the impeller. This, in turn, can lead to different flow patterns and operating characteristics such as head, efficiency, and pressure pulsations of the pump. Although research works provides a wealth of information about the effect of the clocking effect in centrifugal pumps to reveal variations of flow characters like hydraulic losses, pressure pulsations et al, the nature feature of physical boundary conditions downstream of impeller formed by different vane mounted position and its influence on unsteady blade load, flow homogeneity at impeller outlet need to be clarified. This study aims to proposed detailed flow information to investigate the influence of the variation of physical boundary condition on flow instability in impeller and the blade load, pressure pulsation intensity, in order to provide guidance for the proper placement of guide vanes to improve the operating performance of centrifugal pumps. The present work first determines appropriate unsteady impeller position moments by assessing the unsteady power consumption fluctuation of the impeller at different guide vane positions. Subsequently, the impact of the guide vane mounted position on the impeller outlet flow parameters is investigated by means of expanding the impeller outlet turning surface. Finally, the variations in impeller blade load, pressure fluctuation intensity, and radial force at different guide vane positions is examined.

2. NUMERICAL SIMULATION PROCESSION

2.1 Pump Parameters and Mesh Discrete

Table 1 displays the operational and design parameters of the centrifugal pump, encompassing the design flow rate (Q_{des}), design Head (H_{des}), blades number (N_b) for impeller, vane number (N_v) for diffuser, specific speed(n_s) and rotating speed(n). In order to investigate the impact of clocking effects on internal flow characteristics within the centrifugal pump impeller, four distinct combinations of guide vane diffuser and volute configurations were chosen. Figure 1(a) illustrates four relative mounting positions spaced at 18° intervals. The parameter θ_d denotes the relative angular orientation between the vane trailing edge and the volute tongue. Corresponding to the four diffuser mounting positions denoted by θ_{d1}, θ_{d2}, θ_{d3}, and θ_{d4}, which is taken as 0deg,

Table 1 Design parameters of the centrifugal pump

Q_{des} (m^3/s)	H_{des}(m)	N_v	N_b	n_s	n (rpm)
1.11e-2	55	5	6	55	2900

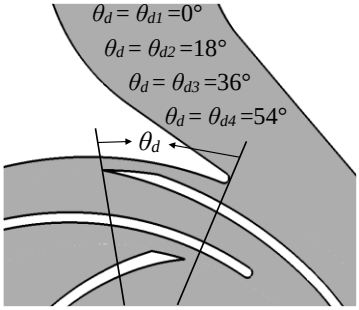

(a) Diffuser position decided

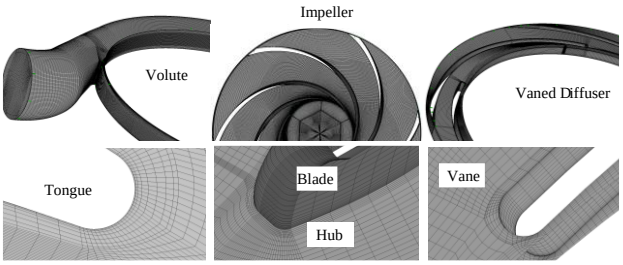

(b) Mesh discrete

Fig. 1 Four diffuser positions and mesh discrete

18deg, 36deg and 54deg, respectively.

Structured grids are used to discretize the computational domain, with enhanced mesh refinement at the boundaries, as shown in Fig. 1(b).

2.2 Numerical Setup

Turbulence modeling is considered with SST *k-ω* model. Since it is both effective in dealing with low Reynolds-number turbulence in the boundary layers and performs well as taking advantage of the *k-ε* formulation in free stream, it is widely used in numerical simulations in centrifugal pumps (Han et al., 2020; Chen et al., 2021; Li et al., 2022). The commercial CFD code, ANSYS CFX is adopted to solve the governing equations. FVM method is used for equation discrete. According to relative research work (Osman et al., 2022), the time-step is set to 0.0000574713s, corresponding to the time it takes for the impeller to rotate by 1°; total pressure inlet and mass flow outlet was adopted; no slip and smooth wall was employed; transient rotor–stator condition was set for rotor-stator interface; convergence criterion was set to 10e-5. The unsteady calculation spans a total of 0.00045977s, which is equivalent to the impeller rotating for 8 revolutions. At this point, the unsteady parameters exhibit strict periodic fluctuations, and the data from the last revolution will be analyzed.

This paper conducts a grid convergence analysis on four different mesh cases with varying numbers under θ_{d4}. The number of grids utilized in each case are shown in Table 2. The comparison of head coefficients on the four different mesh cases is presented in Fig. 2. The results show that there are significant differences between G1 and the other three cases at partial load conditions. As the number of grids increases, the variation in head coefficient decreases gradually. When the number of grids exceeds G2, the variation becomes negligible. The maximum

Table 2 Mesh cases

Mesh case	G1	G2	G3	G4
Element Number	3.631e6	5.572e6	7.871e6	9.764e6

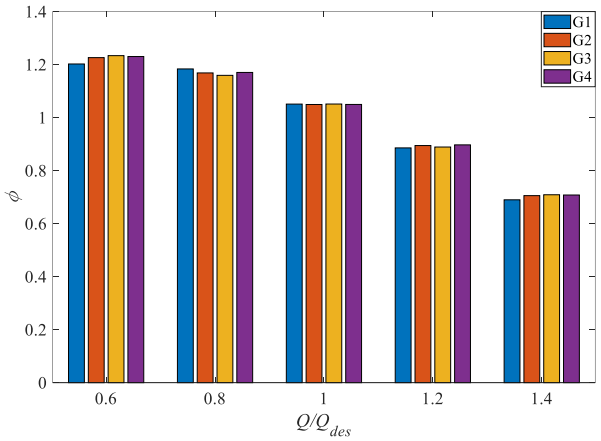

Fig. 2 Mesh convergence study

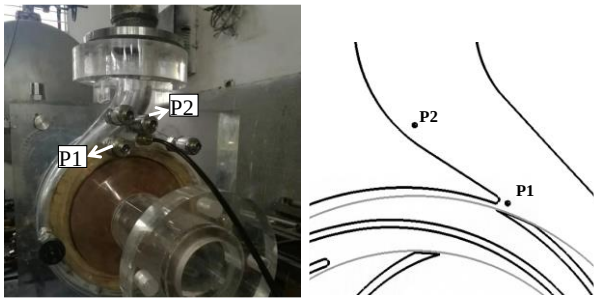

Fig. 3 Experiment setup and schematic diagram of pressure probes

difference in head coefficients between G2 and G4 meshes is less than 2%. Thus G2 mesh is decided for further numerical research.

2.3 Numerical Methods Validation

Figure 3 shows the experiment setup and schematic diagram of pressure monitoring points. Probe P1 is located at tongue where the pressure fluctuation is more typical. P2 is set downstream tongue where the effect of rotor-stator interaction is smaller, and it can serve as a good comparative point. The uncertainty, according to Moffat (1988), involved with pressure measurement is shown in Table 3. It is demonstrated that the uncertainty of pressure measurement is less than 0.9%.

Figure 4 presents a comparison of numerical and experimental head coefficient and amplitude at blade passing frequency (C_{pf}) of pressure at probe P1 and P2 for four different diffuser positions. It shows that the numerical head is higher than the experimental one with the difference within 5% over operating flow rates. At overload conditions, the deviation between the numerical and experimental head coefficient curves is more pronounced compared to that at partial load conditions. The increase in head with flow rate observed in the numerical simulations aligns with the trends seen in the

Table 3 Uncertainty analysis of pressure measurement

Sensor	Pressure Range/MPa	Accuracy/%	Minimum test value/MPa	Uncertainty /%
Absolute pressure	0-0.12	0.25	0.0917	0.3417
Gauge pressure	0-0.5	0.25	0.0928	0.8289

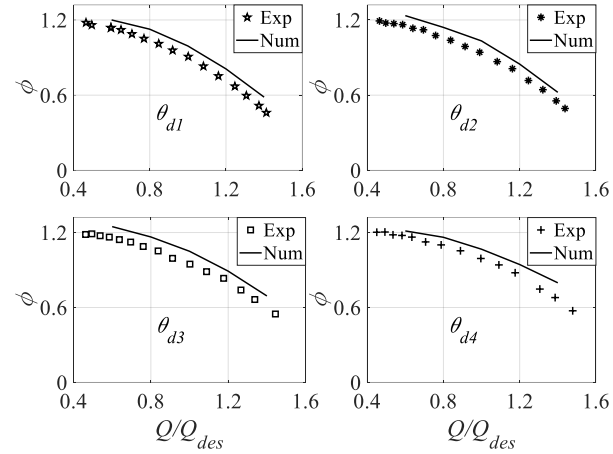

(a) Head coefficient

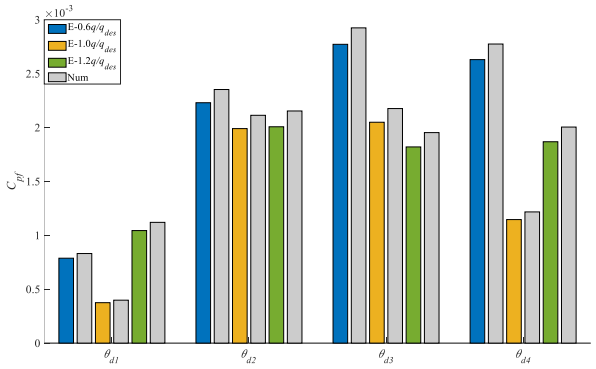

(b) C_{pf} at P1

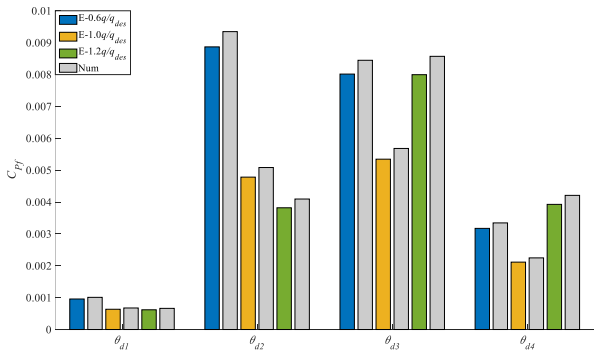

(c) C_{pf} at P2

Fig. 4 Numerical setup validation

experiments conducted with varying diffuser positions. The difference of C_{pf} between experiments and numerical simulations is minimal, with the largest variance being under 4%, irrespective of flow rate and diffuser positions. The spatial positions of pressure probes in numerical simulations may differ from those in experiments due to measurement errors and other factors. This discrepancy contributes to the variations between the calculated and experimental values. In general, there is good agreement between the numerical calculations and experimental results. Therefore, we consider numerical simulations reliable for predicting the fluid field inside the pump.

3. RESULTS AND DISCUSSION

As the impeller rotates, shaft power transforms into mechanical energy for the fluids. The power consumption of the impeller depends on the blade load, influenced by the flow field within the impeller. Figure 5(b-e) shows instantaneous value of power consumption during a single impeller rotation. The power consumption is evaluated using Equation 1, where M and n represent torque and rotating speed in N/m and rpm, respectively; A_2, u_2 represents the area of impeller outlet surface and the speed of trailing edge in m^2 and m/s, respectively. The figure indicates that the impact of rotor-stator interactions on power consumption at various flow rates is consistent, as indicated by the fact that the instantaneous power consumption reaches maximum or minimum values at the same impeller position (T1 and T2) regardless of the flow rate. However, the peak-to-valley amplitude increases with higher flow rates. Within one-sixth of a revolution, there are five peaks and valleys due to impeller-vane interactions, visualized by red lines. These interactions contribute to fluctuations in power consumption. Additionally, the peak values of power consumption fluctuations vary significantly based on the interactions between the blade and different vane leading edges.

Figure 5(f-g) display the power consumption frequency domain for one impeller rotation for four diffuser positions at two flow rates, 0.8 Q/Q_{des} and 1.2 Q/Q_{des}. The dominating frequency observed is the blade passing frequency (f_b) and its harmonics, suggesting a notable influence of impeller-vane interaction on power consumption. Peaks at harmonics of f_b signify the existence of fluctuating flow phenomena attributed to impeller-vane interaction

The amplitude at the dominant frequency increases as the flow rate increases for a specific diffuser position. When the diffuser position changes from θ_{d1} to θ_{d4} with a constant flow rate, the amplitude decreases. In general, the fluctuation intensity tends to increase with increasing flow rate and exhibit a monotonic behavior as the diffuser position changes. Power consumption fluctuations decrease as the vane D1 trailing edge moves away from the tongue, reducing impeller-vane interactions. Therefore, it is possible that the fluctuation intensity shows a monotonic decreasing trend as the vane moves away from the tongue, but it depends on the specific configuration of the tongue and vanes. This is because the impeller blade-vane interaction mechanisms change with the diffuser position, leading to different levels of power consumption fluctuations. The distance of vane D1 trailing edge from the tongue is not the sole factor

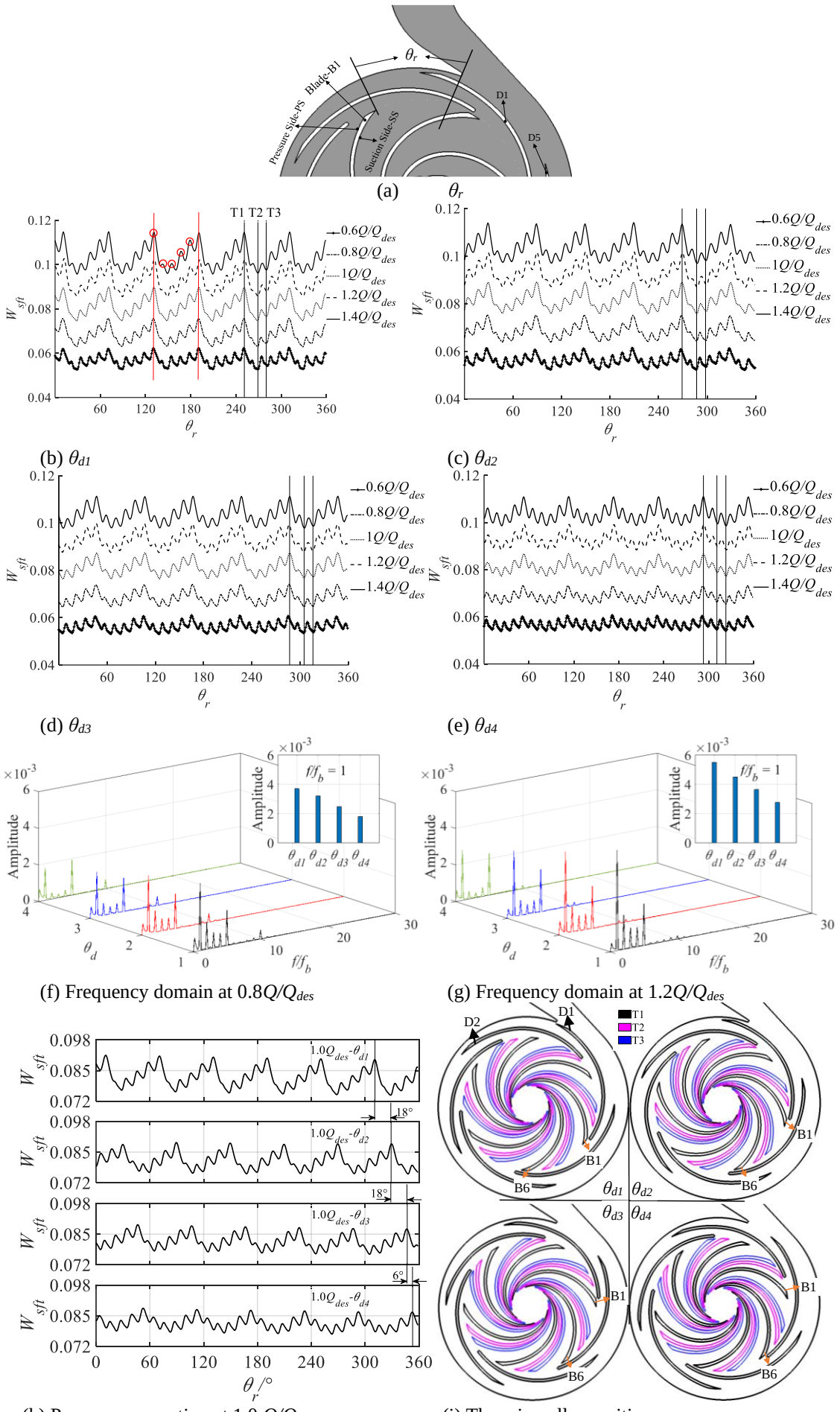

Fig. 5 Power consumption and time step decided

affecting fluctuation intensity. As vane D1 moves away from the tongue, vane D5 approaches it, potentially increasing fluctuation intensity based on their angular distance from the tongue. As a result, the fluctuation intensity conceivable likely increase depending on the angular distance of vane D5 from tongue.

Figure 5(h) shows instantaneous power consumption at 1.0 Q/Q_{des} under four diffuser position. It is shown that the impeller's power consumption curve exhibits similarities, with an 18° phase difference between θ_{d1}-θ_{d3}, reflecting the angular variance in vane positions. However, a 6° phase difference between θ_{d3} and θ_{d4}, independent of the angular position difference of the guide vanes, indicates a shift in the impeller blade-vane interaction mechanism as vane D1 moves away from the tongue and vane D5 approaches it. Figure 5(i) presents three impeller positions, and when the vane is mounted at θ_{d1}, blade B1 is in proximity to vane D1 at T1, which is similar to the situation when the vane is mounted at θ_{d2}-θ_{d3}. However, when the vane is positioned at θ_{d1}, blade B1 is in proximity to vane D1 at T1, resembling the situation with vane positions at θ_{d2}-θ_{d3}. Conversely, with the vane at θ_{d4}, blade B6 is near vane D5 at T1, indicating a distinct impeller blade-vane interaction of strongest undergoes.

$$W_{sft} = \frac{2\pi * Mn/60}{u_2 * A_2 * 0.5 * \rho * u_2^2} \tag{1}$$

The impeller blades transform the shaft power into mechanical energy of the fluid through surface pressure during rotation. Therefore, the characteristics of the pressure field can be reflected in the variation of the work done by the blades. The calculation for the work done by each blade is as follows:

$$W_B = \frac{2\pi * M_B n/60}{u_2 * A_2 * 0.5 * \rho * u_2^2} \tag{2}$$

Where, M_B stands for the torque on blade in N/m.

Figure 6(a-d) shows the instantaneous curves of work done by each blade during one impeller rotation at different diffuser positions under 1.0Q_{des}. The curves show consistent fluctuations characters at constant diffuser mounted position, with a 60° phase difference reflecting the angular separation between adjacent blades. Five peaks are observed due to impeller blade-vane interaction, with one peak significantly larger than the others, suggesting a stronger impeller blade-vane interaction for the corresponding blade at that position. As the diffuser position changes from θ_{d1} to θ_{d4}, the peak value of work done by each blade decreases monotonically, indicating that the diffuser position significantly affects the impeller blade-vane interaction. It is important to note that the power consumption reaches its maximum value where a peak value of work done by the blade occurs.

When the vane is mounted at θ_{d1}-θ_{d3}, the work done by impeller blade B1 attains its maximum value at T1 and a local peak value at T2. Similarly, the work done by impeller blade B6 reaches its first peak value at T1 and a local secondary peak value at T2 when the vane is mounted at θ_{d4}.

Figures 6(e)-(f) demonstrate the instantaneous work performed by blade B1 at θ_{d1} and by blade B6 at θ_{d4} under varying flow rates. The figure demonstrates that under overload conditions, the work done by the blade reaches its maximum value during one impeller rotation at T1. In comparison, the work done by the blade attains its local valley value under partial load condition. Which indicates that the impeller blade-vane interaction is affected significantly by flow rate. Moreover, the five peaks of B1 differ significantly in magnitude, indicating that the strength of interactions between B1 and different vanes is distinct, despite the impeller and diffuser being strictly symmetric. Consequently, different physical boundaries formed by guide vanes and volute significantly affect the flow field in the upstream components under different guide vane positions. This situation is evidently weakened when the diffuser is mounted at θ_{d4}.

In addition, Fig. 6(g) illustrates the work done by B1 at three impeller position for θ_{d4}. The comparison indicates that as the trailing edge of vane D1 moves far away from the tongue, while vane D5 is approaching the tongue, there is a variation in the impeller blade-vane interaction mechanism. At T1 for θ_{d4}, it is not blade B1 but, rather, the stronger interaction occurs for impeller blade B6 as shown in the figure. Figure 6(h) illustrates the work done by the blade at different diffuser positions corresponding to the impeller position. Based on the analysis, it can be concluded that, given the strict symmetry of the impeller and diffuser, the physical boundary conditions formed by the volute and diffuser under different positions lead to significant differences in the flow field within the diffuser passages, thereby causing distinct flow fluctuations in the impeller passages. Thus, θ_{d4} should be the optimized position for the diffuser among the four positions.

Figure 7 illustrates the pressure coefficient distributions on the pressure and suction sides of blade B1 at T1 and T2 for position θ_{d1}. It can be observed that as the impeller rotates from T1 to T2, the pressure on both the pressure and suction sides of B1 increases for 0.8Q/Q_{des}, and decreases for 1.0Q/Q_{des} and 1.2Q/Q_{des}, especially at the blade outlet region, as indicated by circle marks. Under overload conditions, the pressure load on the pressure side decreases more steeply than that on the suction side, resulting in a decrease in work done by the blade. Under partial load conditions, the pressure load on the pressure side increases more sharply than that on the suction side, leading to an increase in work done by the blade. The pressure load undergoes a significant change at the blade outlet region compared to the leading and middle regions of the blade, suggesting that the angular position of the vane has a greater effect on the flow field near the impeller outlet than in the internal region of the impeller.

Figure 8 displays the pressure coefficient patterns on both sides of the downstream channel B6 at location θ_{d4}, captured at two different time points, T1 and T2. The pressure exerted on the blade surface fluctuates in accordance with time and flow rate, akin to B1 at θ_{d1}, yet the pressure fluctuations are significantly less pronounced

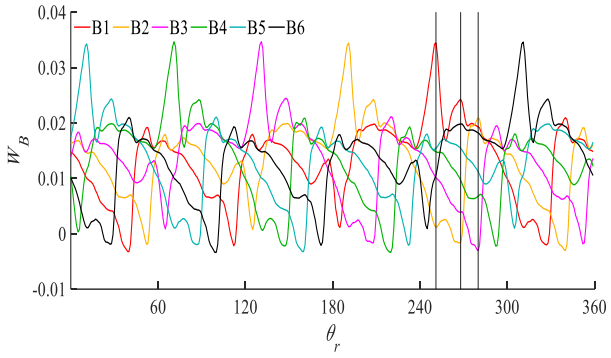

(a) Work done by blade at θ_{d1} for $1.0Q/Q_{des}$

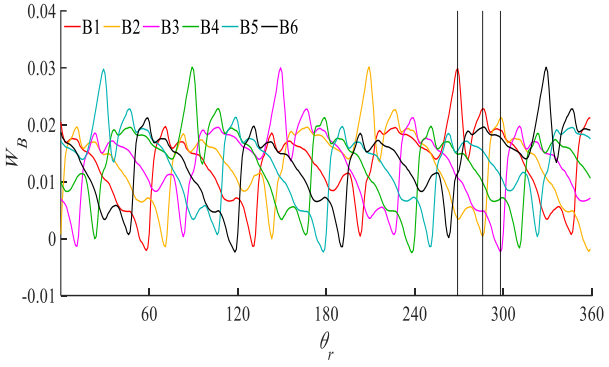

(b) Work done by blade at θ_{d2} for $1.0Q/Q_{des}$

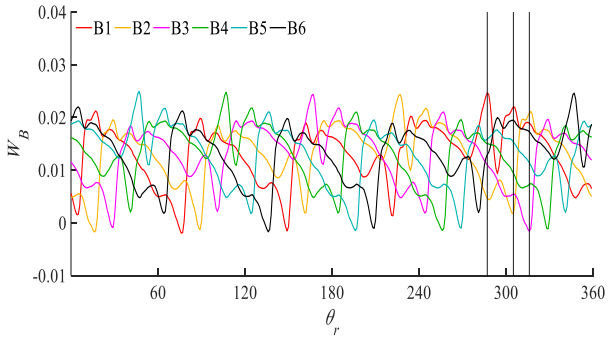

(c) Work done by blade at θ_{d3} for $1.0Q/Q_{des}$

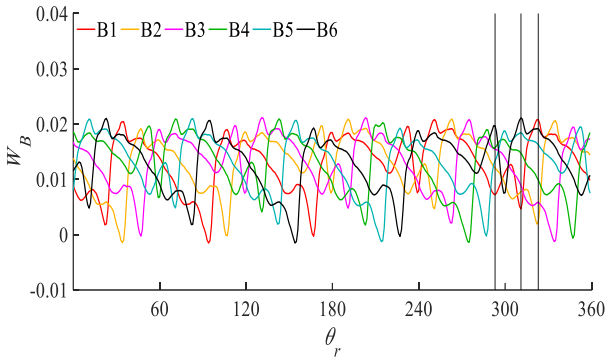

(d) Work done by blade at θ_{d4} for $1.0Q/Q_{des}$

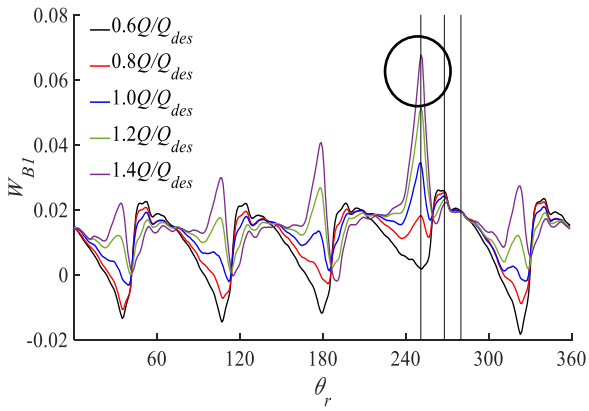

(e) Work done by impeller blade B1 under θ_{d1}

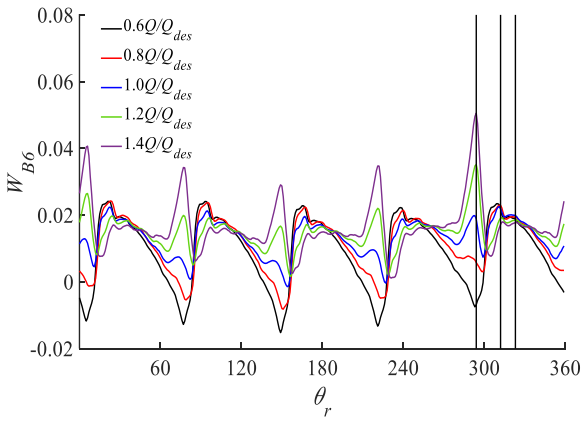

(f) Work done by impeller blade B6 under θ_{d4}

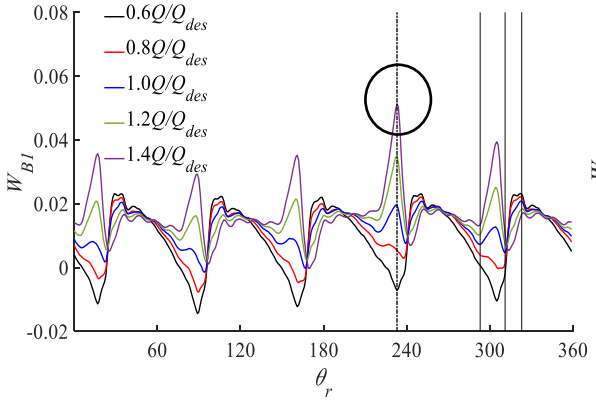

(g) Work done by impeller blade B1 under T1-T3 for θ_{d4}

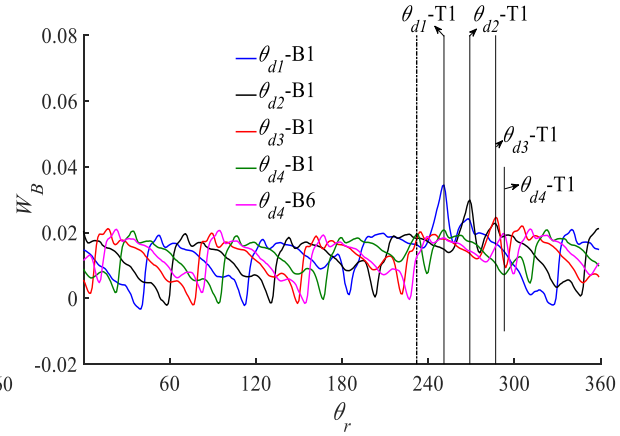

(h) Work done by B1 at different θ_d and B6 at θ_{d4}

Fig. 6 Work done by blade during one impeller rotation

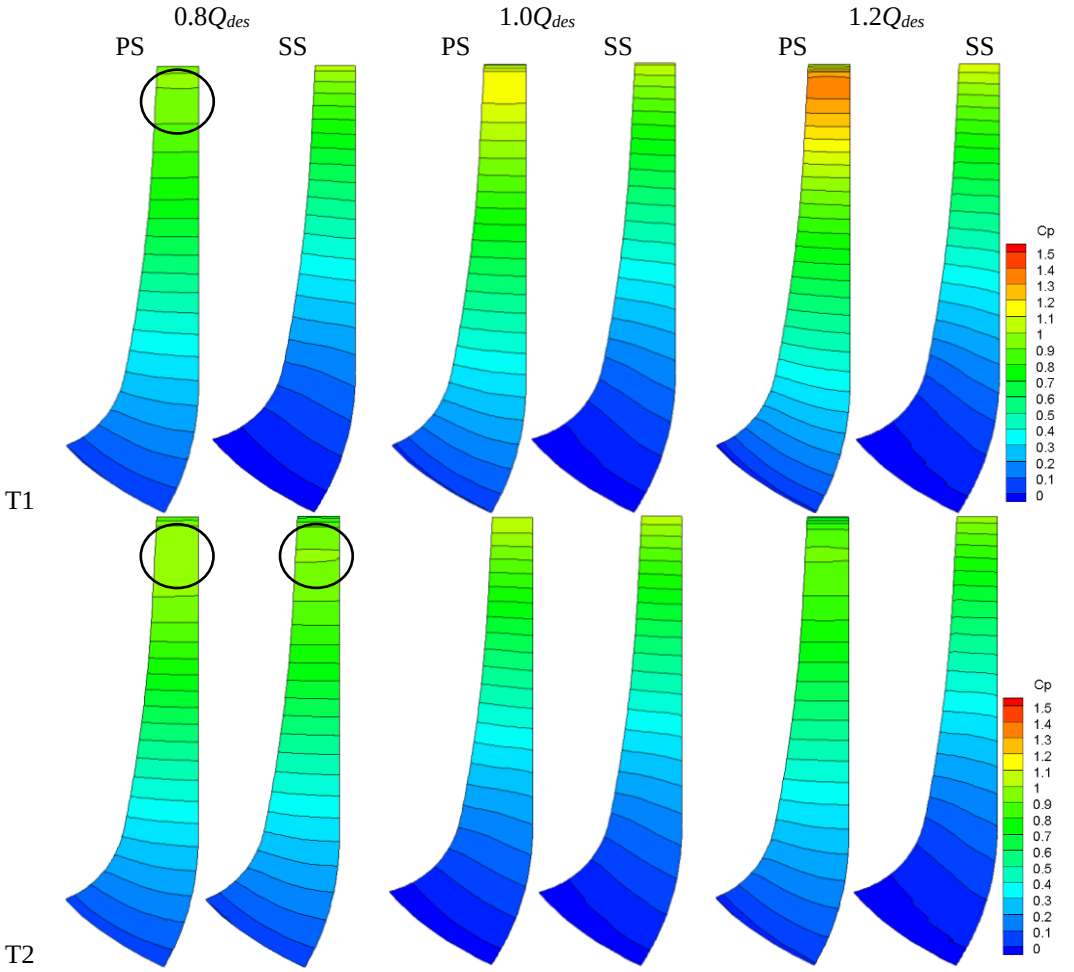

Fig. 7 blade load of blade B1 at T1 and T2 for θ_{d1}

than those at B1 at θ_{d1}. Positioning the diffuser at θ_{d4} seems to mitigate the influence of the diffuser's angular placement on the flow field adjacent to the impeller's exit. The arrangement results in a more consistent flow pattern, attributable to the physical constraints imposed by the volute and diffuser at θ_{d4}.

Figure 9(a-b) illustrates the radial velocity and flow angle distribution at different time instances within the impeller diffuser clearance for four diffuser positions under $0.8Q/Q_{des}$ and $1.2Q/Q_{des}$. As the clearance is very narrow (0.5mm), the distribution is applicable to both the impeller outlet and the diffuser inlet. In the figure, black lines denote contour lines with zero value; grey lines mark the trailing edge of the impeller blade's pressure surface, and white lines indicate the leading edge of the vane blade. The variable θ denotes the angular position relative to the tongue. The figure illustrates that the pattern of flow angle distribution mirrors that of radial velocity, where negative flow angles are associated with negative radial velocities. Since the interval of diffuser position is 18°, the distribution under different θ_d exhibits a phase difference of 18° for θ_{d1}-θ_{d3} and 6° for θ_{d3}-θ_{d4} as preceding analysis, however, the trend of distribution remains similar. As mentioned earlier, when the vane is placed at θ_{d4}, the strongest impeller blade-vane interaction occurs at vane D5 rather than D1. At this point, the phase difference is different from that of other θ_d, as indicated by the red dashed line in the figure.

The figure indicates that negative radial velocity is present at partial flow rates; however, this phenomenon is not observed during overload conditions. Rotor-stator interactions have a significant impact on the radial velocity at the clearance. As the impeller rotates from T1 to T3, the radial velocity varies sharply. When the impeller blade approaches the vane leading edge, the velocity at the blade trailing edge and vane leading edge increases obviously, as indicated by the black dashed line in the figure. As the blade rotates away from the vane trailing edge, the radial velocity decreases, as shown by the black square in the figure.

Observation reveals that as the impeller blade moves past the vane blade, there is a cyclical pattern of 'positive-negative' radial velocity fluctuations in the space adjacent to the vane blade's leading edge when operating at partial load. Under the condition of $1.2Q/Q_{des}$, the radial velocity varies in the same way as that under $0.8Q/Q_{des}$, except for the absence of "positive-negative" radial velocity fluctuations. This is easily concluded that periodic flow field distortion occurs at the impeller outlet region and vane inlet region due to the effect of rotor-stator interactions when the impeller blade passes the vane blade.

Figure (c) shows the standard deviation (STD) and time-averaged value (AVE) of radial and circumferential velocities over one impeller rotation on the clearance

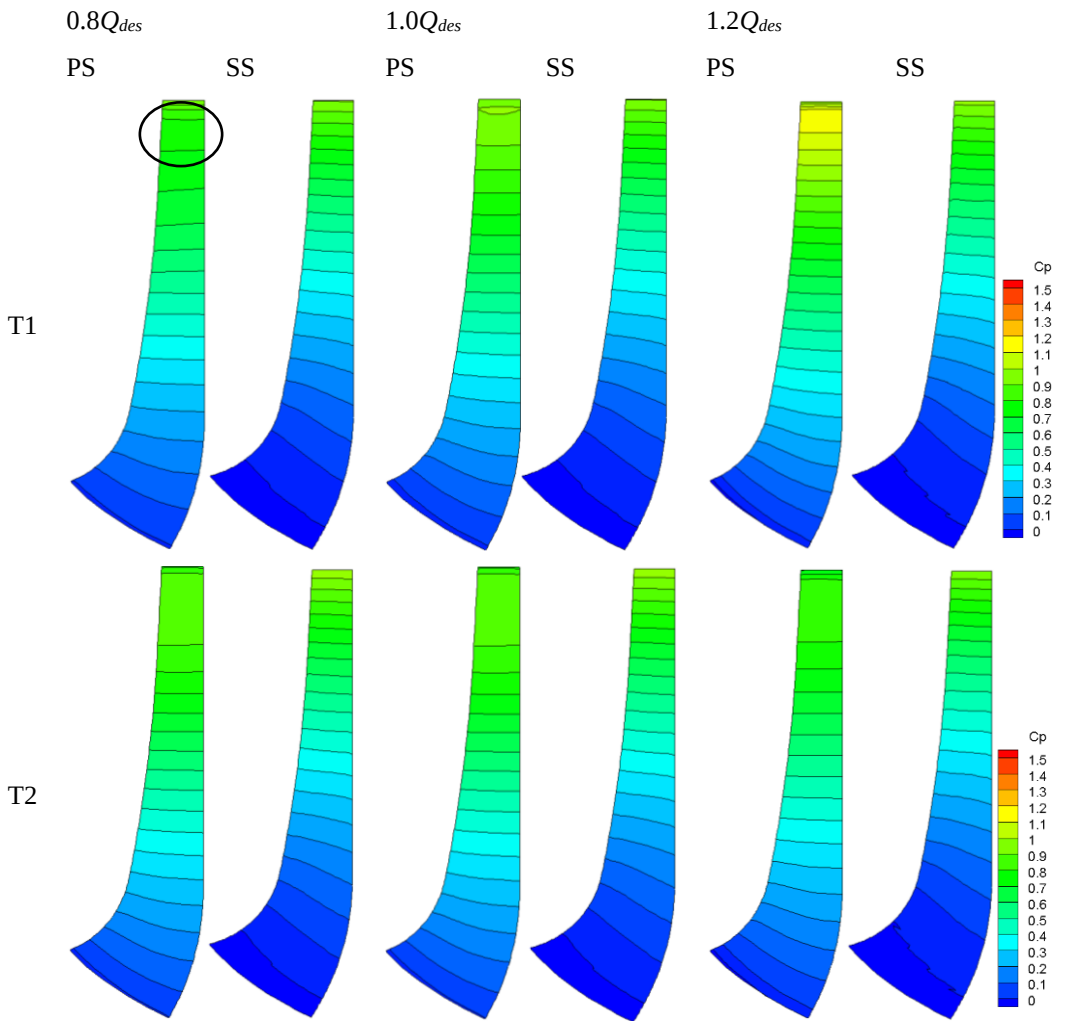

Fig. 8 Blade load of blade B6 at T1 and T2 for θ_{d4}

under the condition of 1.0Q/Q_{des}. It is evident the D1-D2 vane channel area exhibits a greater standard deviation in radial and circumferential velocities compared to other vane channels within the range of θd1 to θd3, signifying more intense fluctuations in the flow field, as denoted by the black square. Note that this situation is more significant under over load condition. When the vane is positioned at θ_{d4}, the standard deviation of radial and circumferential velocities shows more uniformity between different vane channels with a little high at channel D5-D1, suggesting that diffuser position has a significant impact on flow field fluctuation.

The time-averaged data indicates that in the D1-D2 channel, where the standard deviation is larger, both the radial and circumferential velocities are lower compared to the velocities in the other channels. This suggests that there should be stronger flow instabilities or disturbances in this region, which could contribute to the higher fluctuation in velocities and flow rate. As impeller blade sweep past D1 leading edge, the flow rate from the impeller passage must be changes significantly, leading to strong flow instabilities. Figure (d) presents velocity vectors in midsection and radial velocity at diffuser outlet. It can be seen that the clocking effect of the diffuser position on the transient radial velocity is significantly greater than that of the impeller rotation. With the diffuser positioned at the θ_{d1}-θ_{d3} range, the radial velocity in channel D1-D2 is notably reduced. Typically, channel D5-D1 is split by the tongue, exhibiting lower velocities on the left side and higher velocities on the right side. As diffuser is mounted at θ_{d4}, the radial velocity at the channel D1-D2 is obviously increases to be higher than that at θ_{d1}. Thus the flow rate is more evenly distributed among 5 diffuser channels. The fluctuation intensity is reduced.

Figure 9(d) illustrates that at θ_{d1}, the vane channel D1-D2 is positioned against small flow section of the volute, leading to a substantial flow blockage and a decrease in the channel's flow rate. Consequently, this area exhibits a reduced radial velocity, whereas the radial velocity at channel D5-D1, adjacent to the volute outlet, is the highest among all channels. In different diffuser positions, as the D1 trailing edge distances itself from the tongue, the cross-sectional area of the volute that confronts channel D1-D2 expands progressively, thereby alleviating the flow blockage. Meanwhile the radial velocity at channel D5-D1 decreases as it is also affected by the gradually increasing blocking effect. Thus It can be imagined that there is a diffuser position at which the time-averaged flow rate of channel D1-D2 is equal to that of D5-D1, and may result in a more desirable flow field and operating performance.

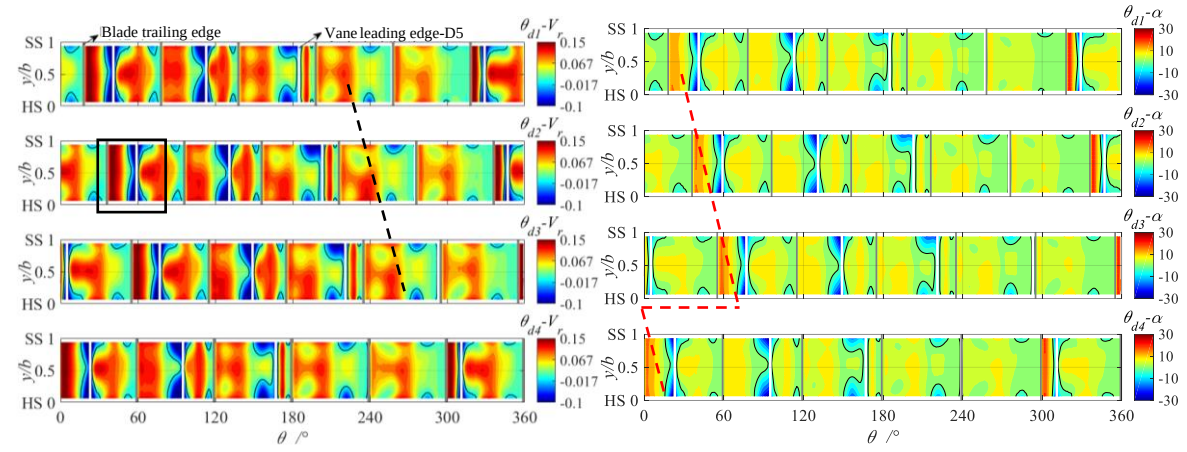

T1

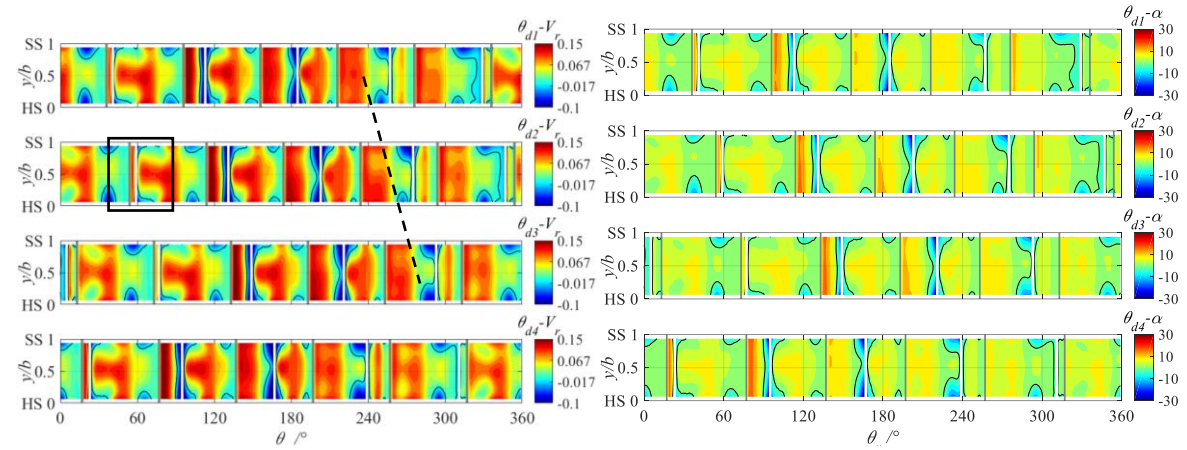

T2

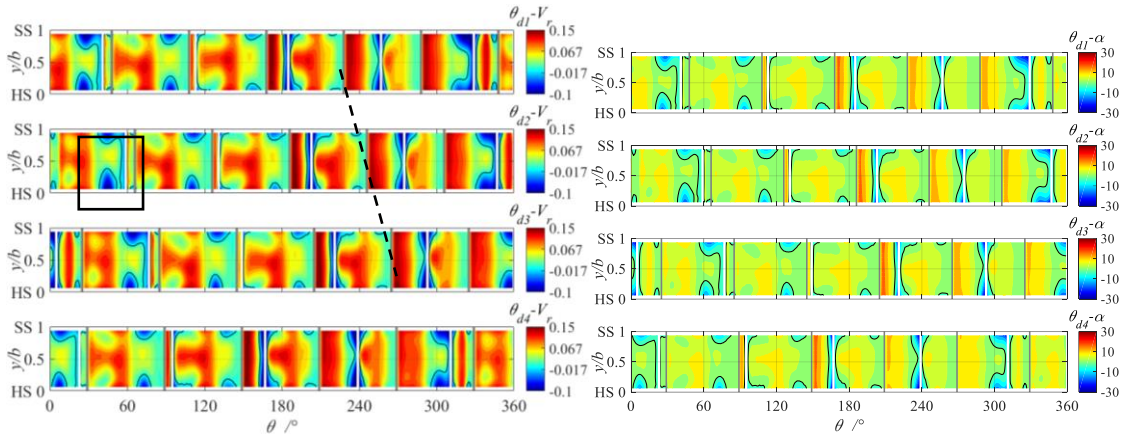

T3

(a) Radial velocity and flow angle at impeller outlet for $0.8Q/Q_{des}$

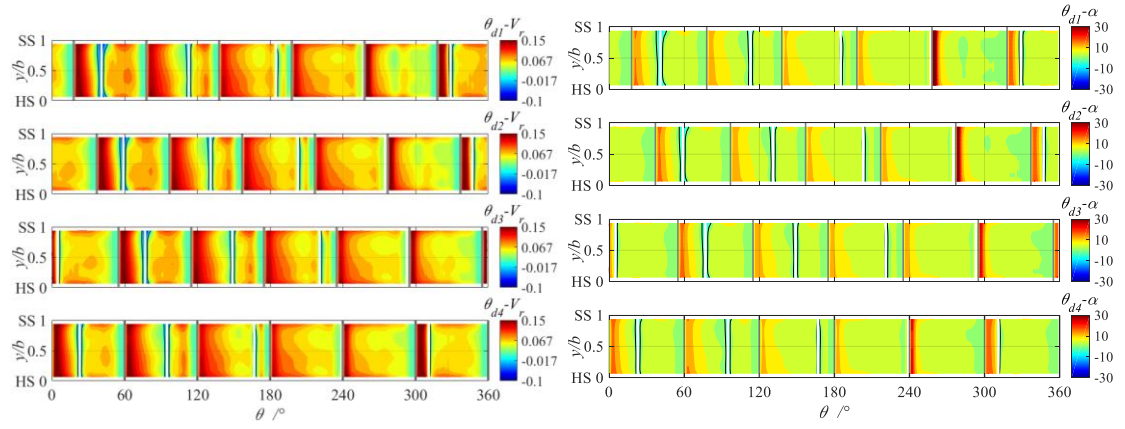

T1

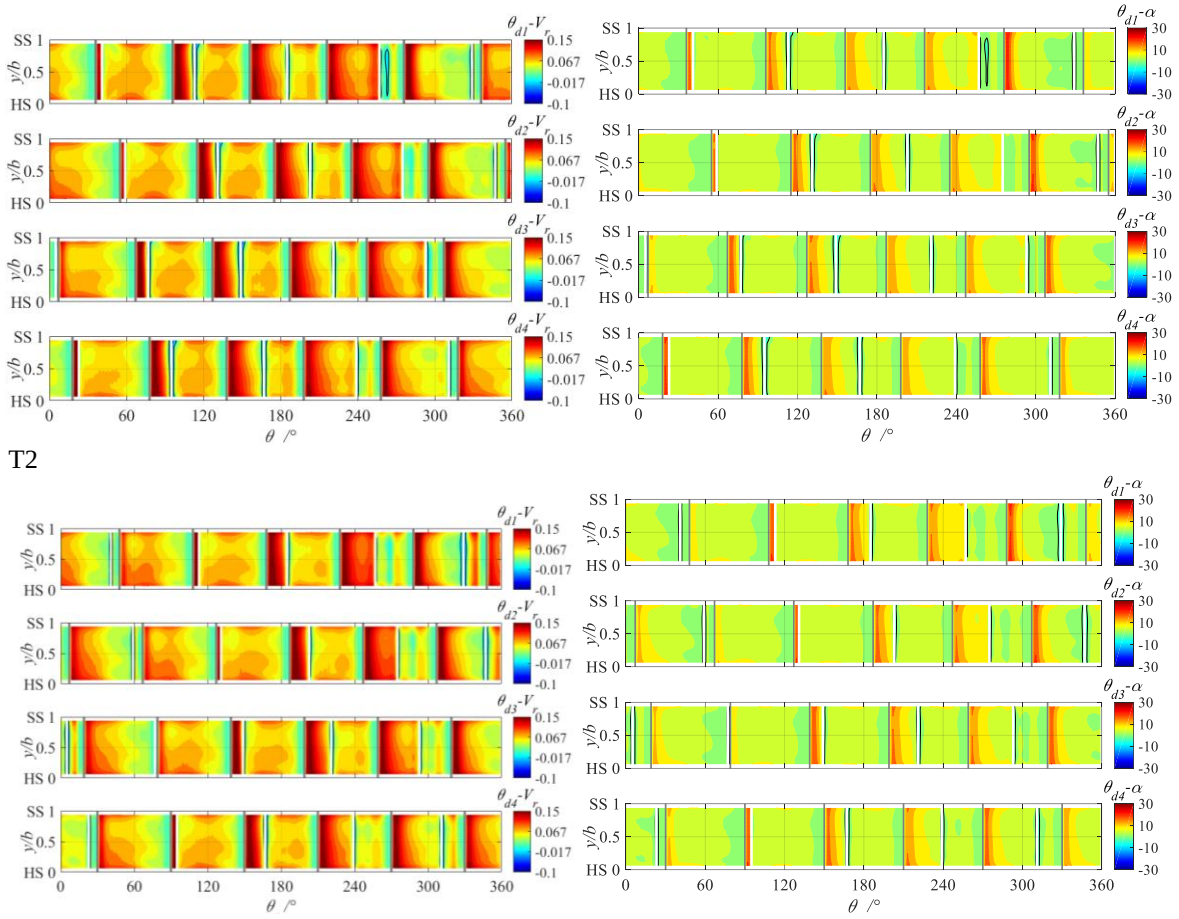

(b) Radial velocity and flow angle at impeller outlet for 1.2Q_{des}

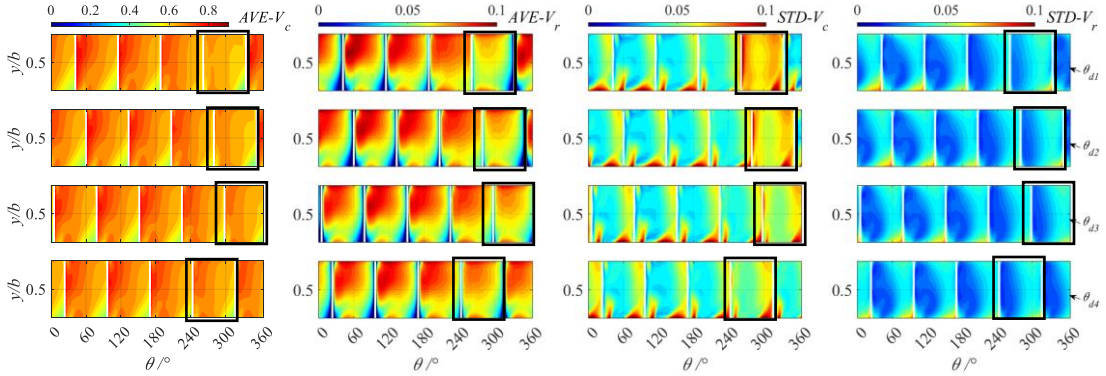

(c) Time-averaged value and standard deviation of radial and circumferential velocity at impeller outlet for 1.0Q/Q_{des}

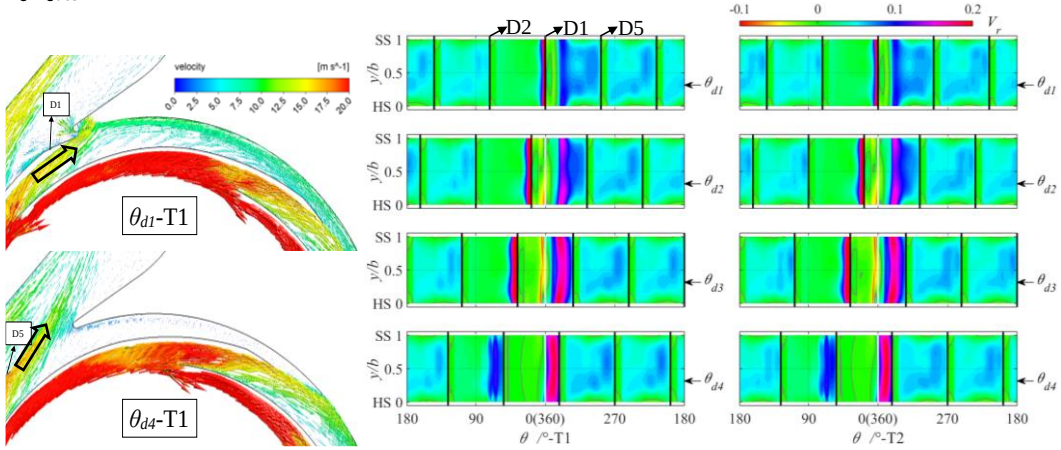

(d) Velocity vectors in midsection and radial velocity at diffuser outlet

Fig. 9 Radial and circumferential velocity and its standard deviation at impeller outlet and diffuser outlet

As vane and impeller is strict symmetric, the asymmetric of volute has a significant impact on the uniformity of flow field, especially the time-averaged flow field in diffuser. The findings imply that the diffuser mounted at position θ_{d4} can balance asymmetry of the volute, bring a better improvement in fluid flow. Therefore, the flow parameter fluctuation is more uniform at θ_{d4} than at θ_{d1}.

Figure 10 displays the blade-to-blade streamline view at different diffuser positions for T1 and T3, under the conditions of $0.8Q/Q_{des}$ and $1.2Q/Q_{des}$. The figure shows the presence of a vortex zone in the latter half of the blade at a flow rate of $0.8Q/Q_{des}$. The vortex area reduces when the blade passes the vane's leading edge and then grows as the blade continues to move away from this edge, as shown by the black arrow. Simultaneously, the vortex core moves outward towards the impeller's outlet, as marked by the red arrow in the figure at time T1. The vortex at the blade nearly dissipates by the time the blade passes the leading edge of D5, as denoted by the ellipses. At the θ_{d4} guide vane position, the temporal changes of the vortex are akin to those observed at θ_{d1}. significantly smaller compared to the vortex at B1 when the guide vanes are at θ_{d1}, as indicated by the red ellipses. At the $1.2Q/Q_{des}$ operating condition, the vortex behavior over time across various guide diffuser positions mirrors that at $0.8\ Q/Q_{des}$. However, the vortex region is more compact at $1.2Q/Q_{des}$ compared to its size at $0.8Q/Q_{des}$.

The figure reveals that the vortex at the blades consistently exhibits a trend of initial growth followed by a decline as the blade nears the leading edge of the guide vanes, particularly at the blade's trailing edge. This leads to intense fluctuation in flow field at blade trailing edge. Figure 10(c) and (d) illustrates the pressure coefficient distribution at flow rates of $0.8Q/Q_{des}$ and $1.2Q/Q_{des}$, respectively. When the blade passes the vane's leading edge, the pressure fluctuations at the blade's trailing edge are more pronounced for θ_{d1} compared to θ_{d4}. Additionally, it is observed that at T1 the pressure at B1 under θ_{d1} is significantly higher than that under θ_{d4}, as indicated by the ellipses.

To evaluate the fluctuations in flow field, standard deviation of pressure (C_{psdv}) is made during one impeller rotation. The formula for calculating C_{psdv} is as follows,

$$\bar{p}(node) = \frac{1}{N}\sum_{j=0}^{N-1} p(node, t_0 + j\Delta t) \tag{3}$$

$$\tilde{p}(node,t) = p(node,t) - \bar{p}(node) \tag{4}$$

$$C_{Psdv} = \frac{\sqrt{\frac{1}{N}\sum_{j=0}^{N-1}\tilde{p}(node, t_0 + j\Delta t)^2}}{0.5\rho u_2^2} \tag{5}$$

Where, $\bar{p}$ is time-averaged pressure, $\tilde{p}$ is the fluctuation component, u_2 is speed of impeller blade trailing edge, t_0 is the starting time, Δt is the time step.

Figure 11 illustrates C_{psdv} at mid-section during one impeller rotation. It can be observed that at position θ_{d1}, the pressure fluctuation within both the volute and the guide vanes intensify with rising flow rates, though they remain relatively minor. At partial flow rates, the pressure fluctuation inside the impeller mainly occurs at the exit area of the pressure side of the blades, as shown by the black circle.

At design flow rates, the pressure fluctuation mainly occurs in a small area at the trailing edge of the impeller and is much smaller than that at low flow rates. At overload flow rates, the pressure fluctuation mainly occurs on the pressure side near the trailing edge of the blades, as depicted by the square. A zone of significant pressure fluctuation emerges at the inlet of guide vane D1, as shown by the red circle. Since the radial velocity at the inlet of the guide vane channel D1-D2 is much smaller than that of other guide vane channels, pressure fluctuations occur as the impeller blades sweep past the vane leading edge of D1, as demonstrated in Fig. 9.

At position θ_{d4}, the distribution of pressure fluctuations inside the impeller from inlet to outlet is similar to that at θ_{d1}, primarily concentrated at the blade's trailing edge. However, the intensity of these fluctuations is notably lower. Additionally, the pressure fluctuation intensity within both the guide vanes and the volute diminishes under partial load conditions. However, it experiences a slight uptick near the tongue during design and overload conditions. with the diffuser positioned at θ_{d4}, the flow field exhibits greater uniformity and reduced fluctuation intensity.

Figure 12 illustrates the time-averaged pressure curve at the impeller outlet for two different guide diffuser positions. As shown, the pressure reaches a maximum and then decreases sharply along the leading edge of the vane for both positions. The peak-to-valley value of the pressure decreases as the flow rate increases. At θ_{d1}, the peak-to-valley value near the inlet edge of guide vane D1 is notably less than that of the other vanes. This difference is due to the lower radial and circumferential velocities at channel D1-D2, which result in higher pressures at this location. When the guide vane is positioned at θ_{d4}, the pressure distribution becomes more periodic over the impeller outlet, and the peak-to-valley value of pressure near the inlet edge of guide vane D5 is slightly lower than that of the other vanes. This is due to the fact that the mean radial and circumferential velocity at channel D5-D1 is only slightly lower than that of other channels. The pressure distribution is more circumferentially symmetric at θ_{d4} than it is at θ_{d1}.

Figure 13(a) shows instantaneous value of the radial force (F) acting on the impeller and its time-averaged and standard deviation at different flow rates under two different guide diffuser positions during one impeller rotation. Figure 13(b) shows frequency domain of radial force. Figure 13(a) shows that the radial force exerted on the impeller exhibits strong periodicity across various flow rates and diffuser positions for strict symmetry of impeller. The radial force under partial load condition is bigger than that under other flow rate, with stronger fluctuation intensity. When vane is placed at θ_{d4}, the radial force and its fluctuation intensity is significantly smaller compared to θ_{d1}.

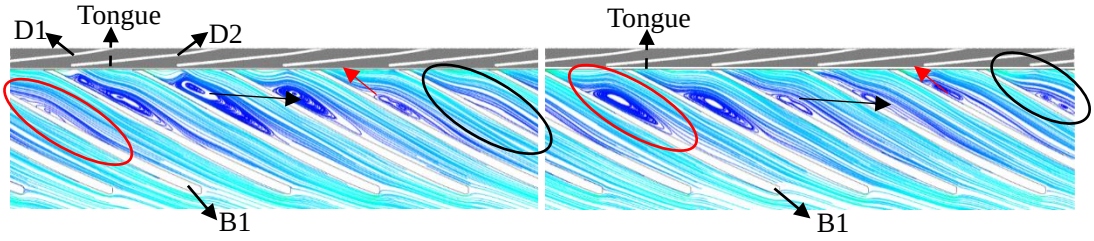

T1 **T3**

i.θ_{d1}

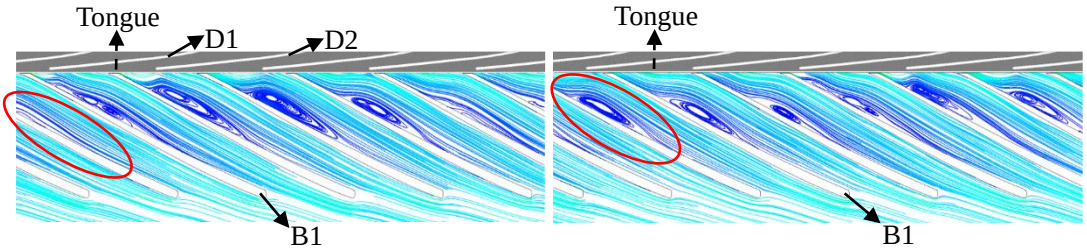

T1 **T3**

ii.θ_{d4}

(a) $0.8Q/Q_{des}$

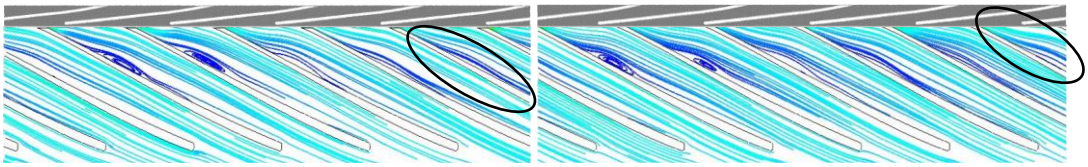

T1 **T3**

i.θ_{d1}

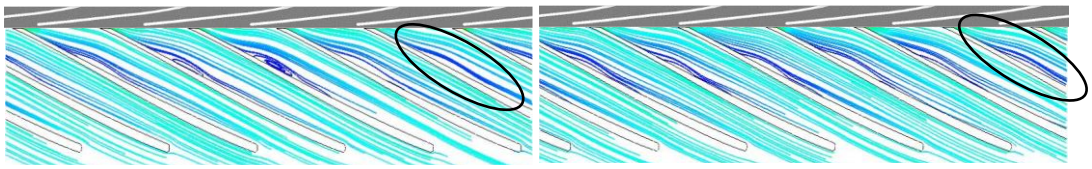

T1 **T3**

ii.θ_{d4}

(b) $1.2Q/Q_{des}$

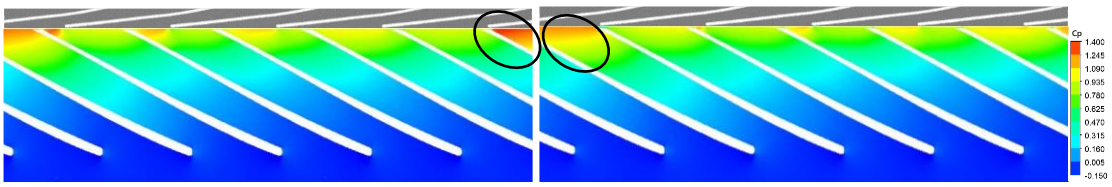

T1 **T3**

i.θ_{d1}

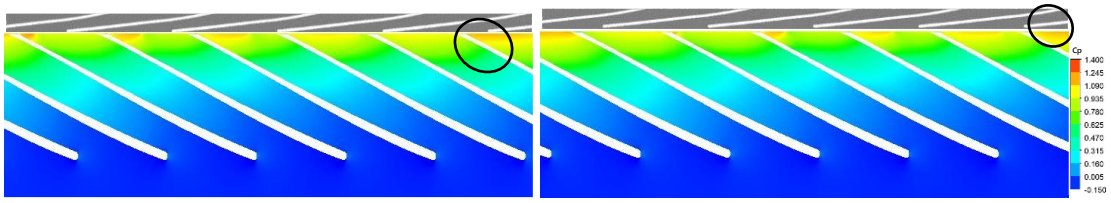

T1 **T3**

ii.θ_{d4}

(c) $0.8Q/Q_{des}$

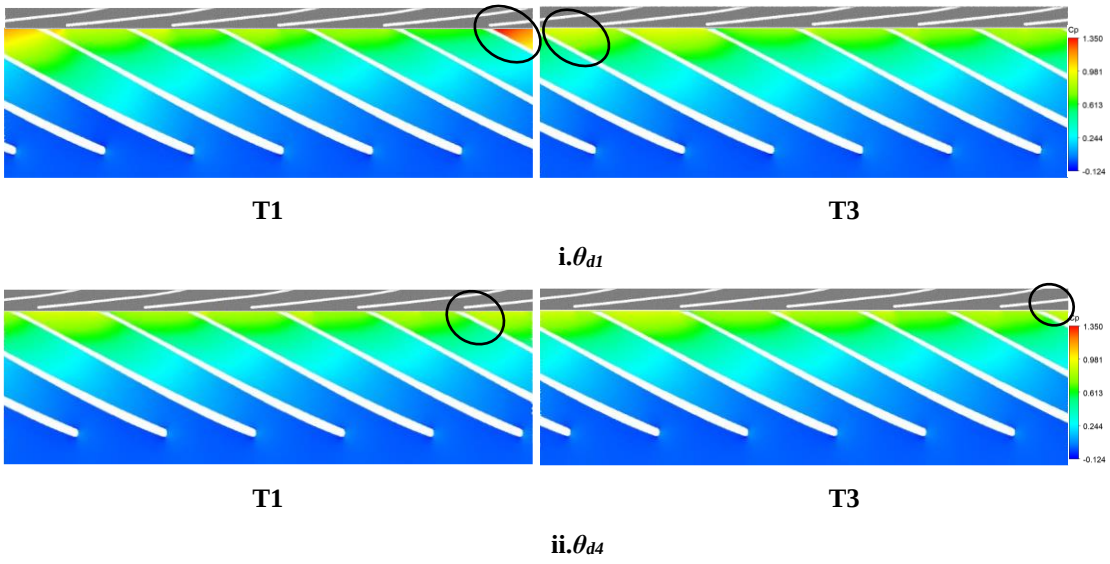

(d) $1.2Q/Q_{des}$

Fig. 10 Stream line and pressure distribution in blade-blade surface at span of 0.5

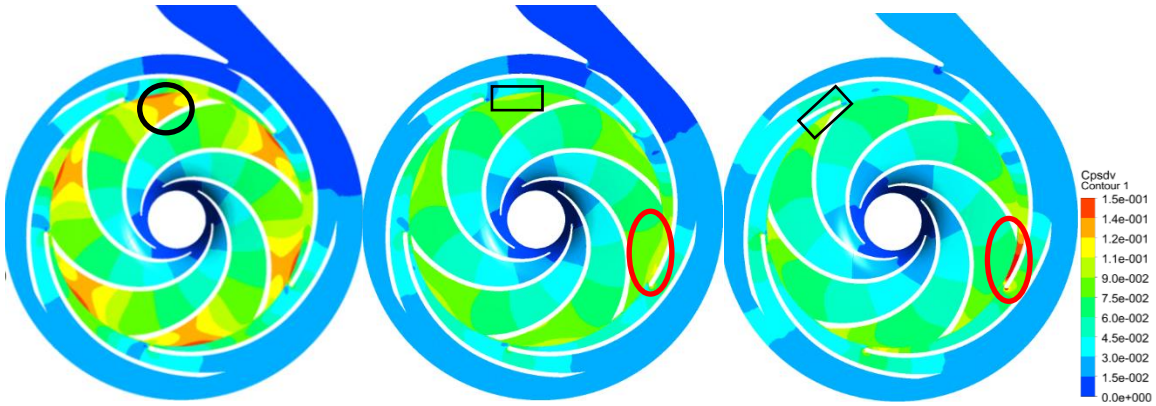

(a) θ_{d1}

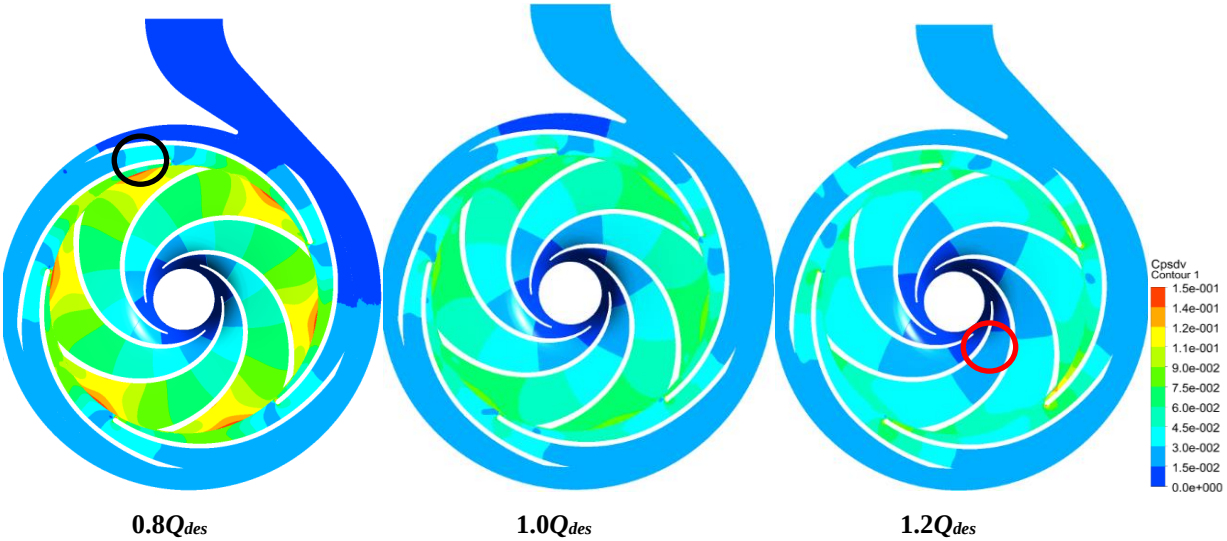

(b) θ_{d4}

Fig. 11 Intensity of pressure pulsation during one impeller rotation under three flow rate for θ_{d1} and θ_{d4}

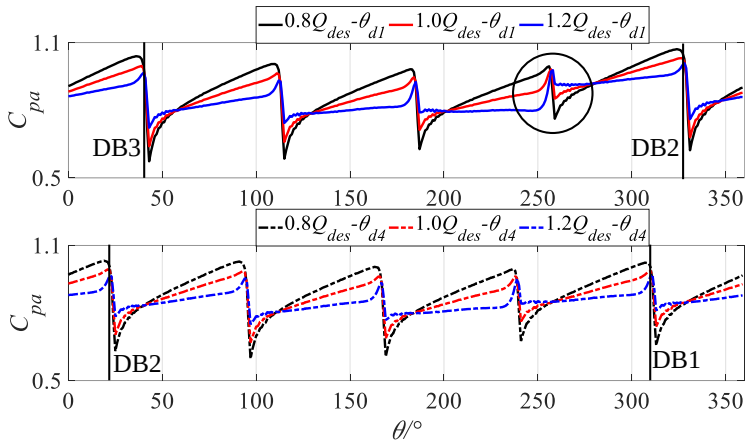

Fig. 12 Time-averaged pressrure at impeller outlet surface at different flow rate for θ_{d1} and θ_{d4}

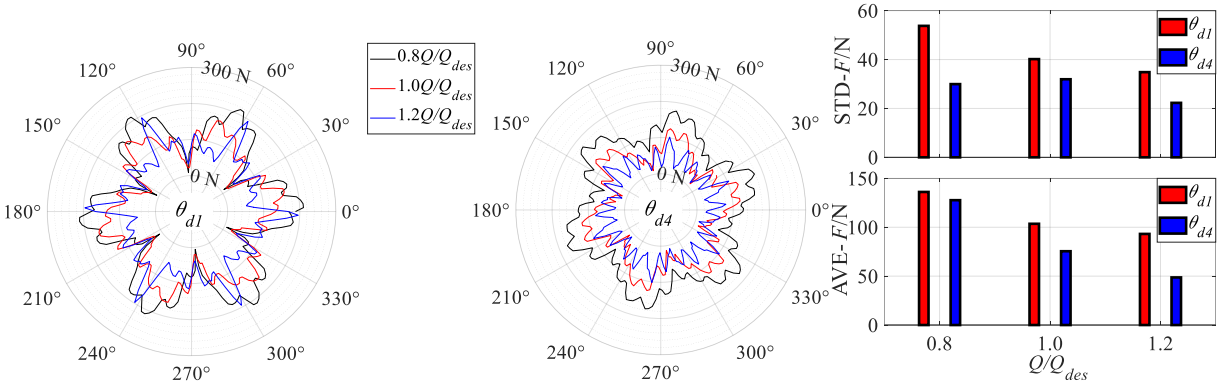

(a) Transient radial force acting on impeller and its standard deviation, time-averaged value

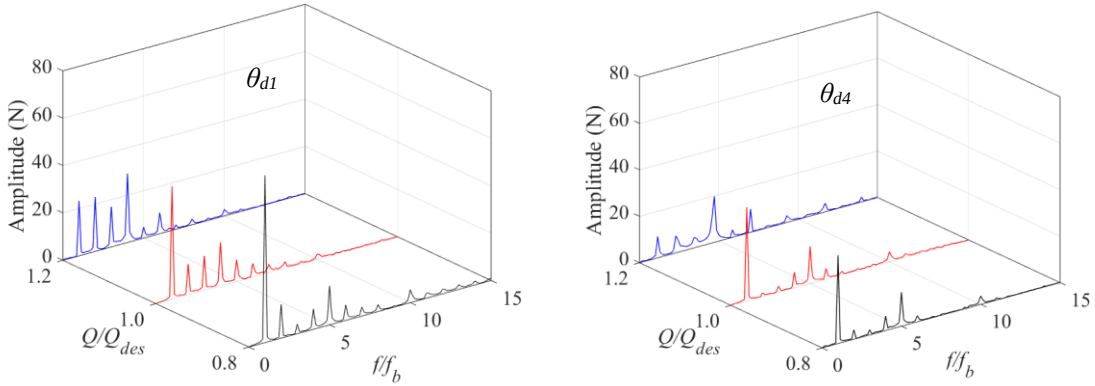

(b) Frequency domain of transient radial force acting on impeller

Fig. 13 Transient radial force acting on impeller and its standard deviation, frequency domain

The placement of the diffuser at θ_{d1} and θ_{d4} has an effect on the radial force acting on the impeller and the dominant frequency of this force. From Fig. 13(b), it can be observed that when the vane is placed at θ_{d1}, the dominant frequency of radial force is the blade passing frequency, with higher amplitude compared to other harmonic frequencies under partial load and design conditions. The amplitude of four times blade passing frequency is slightly higher than other harmonic frequencies with a very small difference. However, with the vane positioned at θ_{d4}, the radial force amplitude is reduced in comparison to θ_{d1}, across all flow rates. The blade passing frequency remains the predominant frequency for radial force, with a distinct amplitude difference compared to other harmonic frequencies under partial load and design conditions. Additionally, at 1.2 Q/Q_{des}, the amplitude at four times the blade passing frequency is notably higher than that of the other harmonic frequencies. Positioning the vane at θ_{d4} improves the flow field and reduces the radial force acting on the impeller, indicating that diffuser position of the θ_{d4} offers greater balancing effectiveness against the volute's asymmetry.

4. CONCLUSION

The present work demonstrates an in-depth investigation of the influence of vane clocking effect on flow fluctuation within the impeller of a centrifugal pump with vaned diffuser. Starting from the fluctuations of the transient external characteristic, typical fluctuation moments are determined to further study the distribution differences of the internal flow field during these moments. Considering the symmetry of the impeller and diffuser, the physical boundary condition formed by the volute and diffuser under different positions should be the dominant impetus for circumferentially inhomogeneous flow since the boundaries change as the diffuser position varies. Therefore, the flow angle, radial velocity, circumferential velocity, and their standard deviation at the clearance between the impeller and diffuser were compared to demonstrate the mechanism of the effect of diffuser position on flow fluctuation within the impeller. The following conclusions were drawn:

(1) During one-sixth impeller revolution, the power consumption of the impeller varies due to impeller blade-vane interaction, resulting in the 5 peaks and valleys. However, the peak value differs in magnitude significantly depending on the intensity of the interaction between impeller blade and different diffuser vanes. When diffuser is mounted at θ_{d1}-θ_{d3}, the strongest interaction occurs at vane D1, whereas at θ_{d4}, the strongest interaction occurs at vane D5, and the difference of peak values is reduced.

(2) As blade sweeps past vane leading edge, the vortex zone at blade changes sharply with diminish and increase. Which leads to significant variation in blade load. The variation of blade load depends on vanes, since the interactions between blade and different vane is quite different. This situation is improved significantly when the diffuser is placed at θ_{d4}.

(3) When the diffuser is set at θd1, with vane D1's trailing edge aligned with the tongue, the channel adjacent suffers blocking effect. Leading to a decrease on the flow rate through the channel. High intensive pressure pulsation occurs at impeller blade trailing edge under partial load condition. In addition, the radial force presents high magnitude and amplitude at blade passing frequency.

(4) As diffuser is mounted at θ_{d4}, the blocking effect within diffuser channel reduces, the flow rate is more evenly distributed among each channel, the interaction intensity at different vane leading edge is more homogeneous. However, there may still be an optimal diffuser position, such as an inflection point, at which the time-averaged flow rate of channel D1-D2 is equal to that of D5-D1. This may lead to an even more desirable flow field and operating performance. Therefore, further research can be done to determine if such an optimal diffuser position exists and how it can be achieved.

ACKNOWLEDGEMENTS

The authors disclosed receipt of the following financial support for the research, authorship, and/or publication of this article: This work was supported by National Natural Science Foundation (grant no. 51809218), the Natural Science Foundation of Shan Dong Province (grant no. ZR2021QE258), Doctoral Foundation of Shandong Jianzhu University (grant no. X21014Z). The supports are gratefully acknowledged.

CONFLICT OF INTEREST

We declare that we do not have any commercial or associative interest that represents a conflict of interest in connection with the work submitted.

AUTHORS CONTRIBUTION

Xiangyuan Zhu: Funding acquisition, Investigation. **Xiaoyu Han:** Writing – original draft, Formal analysis. **Changcheng Xie:** Data curation. **Hao Zhang:** Supervision, Writing – review & editing. **Wei Jiang**: Software

REFERENCES

Arnone, A., Marconcini, M., Pacciani, R., Schipani, C., & Spano, E. (2002). Numerical investigation of airfoil clocking in a three-stage low pressure turbine. *Journal of Turbomachinery*, *124*(1), 61-68. https://doi.org/doi.org/10.1115/1.1425810

Billiard, N., Paniagua, G., & Dénos, R. (2008). Impact of clocking on the aero-thermodynamics of a second stator tested in a one and a half stage HP turbine. *Journal of Thermal Science*, *17*(002), 97-110. https://doi.org/10.1007/s11630-008-0097-7

Chen, J., Shi, W., & Zhang, D. (2021). Influence of blade inlet angle on the performance of a single blade centrifugal pump. *Engineering Applications of Computational Fluid Mechanics*, *15*(1), 462-475. https://doi.org/10.1080/19942060.2020.1868341

Dorney, D. J., Sharma, O. P., & Gundy-Burlet, K. L. (1998). Physics of airfoil clocking in a high-speed axial compressor. *International Journal of Turbo & Jet Engines*, *15*(4), 12pages, Article 98-GT-082, V001T01A024. https://doi.org/doi.org/10.1115/98-GT-082

Ennouri, M., Kanfoudi, H., Bel Hadj Taher, A., & Zgolli, R. (2019). Numerical flow simulation and cavitation prediction in a centrifugal pump using an SST-SAS turbulence model. *Journal of Applied Fluid Mechanics*, *12*(1), 25-39. https://doi.org/doi.org/10.29252/JAFM.75.253.28771

Gong, J., Luo, W. Z., Wu, T. C., & Zhang, Z. Y. (2022). Numerical analysis of vortex and cavitation dynamics of an axial-flow pump. *Engineering Applications of Computational Fluid Mechanics*, *16*(1), 1921-1938. https://doi.org/doi.org/10.1080/19942060.2022.2122570

Gu, Y., Pei, J., Yuan, S., Wang, W., Zhang, F., Wang, P., Appiah, D., & Liu, Y. (2019). Clocking effect of

vaned diffuser on hydraulic performance of high-power pump by using the numerical flow loss visualization method. *Energy*, *170*, 986-997. https://doi.org/doi.org/10.1016/j.energy.2018.12.204

Guan, H., Jiang, W., Wang, Y., Hou, G., Zhu, X., Tian, H., & Deng, H. (2021). Effect of vaned diffuser clocking position on hydraulic performance and pressure pulsation of centrifugal pump. *Proceedings of the Institution of Mechanical Engineers, Part A: Journal of Power and Energy*, *235*(4), 687-699. https://doi.org/doi.org/10.1177/09576509209672

Han, C. Z., Xu, S., Cheng, H. Y., Ji, B., & Zhang, Z. Y. (2020). LES method of the tip clearance vortex cavitation in a propelling pump with special emphasis on the cavitation-vortex interaction. *Journal of Hydrodynamics*, *32*(6), 1212-1216. https://doi.org/doi.org/10.1007/s42241-020-0070-9

Hongyu, G., Wei, J., Yuchuan, W., Hui, T., Ting, L., & Diyi, C. (2021). Numerical simulation and experimental investigation on the influence of the clocking effect on the hydraulic performance of the centrifugal pump as turbine. *Renewable Energy*, *168*, 21-30. https://doi.org/doi.org/10.1016/j.renene.2020.12.030

Huber, F. W., Johnson, P. D., Sharma, O. P., Staubach, J. B., & Gaddis, S. W. (1996). Performance improvement through indexing of turbine airfoils: part 1 - experimental investigation. *Journal of Turbomachinery*(4), 118. https://doi.org/doi.org/10.1115/1.2840918

Jiang, W., Li, G., Liu, P. F., & Fu, L. (2016). Numerical investigation of influence of the clocking effect on the unsteady pressure fluctuations and radial forces in the centrifugal pump with vaned diffuser. *International Communications in Heat and Mass Transfer*, *71*, 164-171. https://doi.org/doi.org/10.1016/j.icheatmasstransfer.2015.12.025

Lai, F., Zhu, X., Duan, Y., & Li, G. (2020). Clocking effect in a centrifugal pump with a vaned diffuser. *Modern Physics Letters B*, *34*(26), 2050286-2050281-2050219. https://doi.org/doi.org/10.1142/S0217984920502863

Li, H., Han, Y., Shi, W., Tiganik, T., & Zhou, L. (2022). Automatic optimization of centrifugal pump based on adaptive single-objective algorithm and computational fluid dynamics. *Engineering Applications of Computational Fluid Mechanics*, *16*(1), 2222-2242. https://doi.org/10.1080/19942060.2022.2143901

Li, W., Yu L., Ji L., Li H., Li S., Chen Y., & Yang Q. (2024a). Effect of circumferential spokes on the rotating stall flow field of mixed-flow pump. *Energy, 290* (2024), 130260. https://doi.org/10.1016/j.energy.2024.130260

Li, W., Yang Q., Yang Y., Ji L., Shi W., & Ramesh, A. (2024b). Optimization of pump transient energy characteristics based on response surface optimization model and computational fluid dynamics. *Applied Energy,* 362, 123038. https://doi.org/10.1016/j.apenergy.2024.123038

Ma, Y., Luo, H., Zhang, Z., Zhou, S., & Deng, H. (2017). Numerical modeling of dynamic characterics for combined valves in multiphase pump. *Engineering Applications of Computational Fluid Mechanics*, *11*(1), 328-339. https://doi.org/doi.org/10.1080/19942060.2017.1292409

Moffat, R. J. (1988). Describing the uncertainties in experimental results. *Experimental Thermal and Fluid Science*, *1*(1), 3-17. https://doi.org/10.1016/0894-1777(88)90043-X

Osman, F. K., Zhang, J., Lai, L., Kwarteng, A. (2022). Effects of turbulence models on flow characteristics of a vertical fire pump. *Journal of Applied Fluid Mechanics* *15*(6): 1661-1674. https://doi.org/10.47176/JAFM.15.06.1303

Posa, A. (2021). LES investigation on the dependence of the flow through a centrifugal pump on the diffuser geometry. *International Journal of Heat and Fluid Flow*, *87*, 108750. https://doi.org/doi.org/10.1016/j.ijheatfluidflow.2020.108750

Qu, W., Tan, L., Cao, S., Wang, Y., & Xu, Y. (2016). Numerical investigation of clocking effect on a centrifugal pump with inlet guide vanes. *Engineering Computations*, *33*(2), 465-481. https://doi.org/10.1108/EC-12-2014-0259

Rogovyi, A., Korohodskyi, V., & Medvediev, Y. (2021). Influence of Bingham fluid viscosity on energy performances of a vortex chamber pump. *Energy*, *218*, 119432. https://doi.org/doi.org/10.1016/j.energy.2020.119432

Shi, L., Yuan, Y., Jiao, H., Tang, F., Cheng, L., Yang, F., Jin, Y., & Zhu, J. (2021). Numerical investigation and experiment on pressure pulsation characteristics in a full tubular pump. *Renewable Energy*, *163*, 987-1000. https://doi.org/https://doi.org/10.1016/j.renene.2020.09.003

König, S., Stoffel, B., & Taher Schobeiri, M. (2009). Experimental investigation of the clocking effect in A 1.5-stage axial turbine-part 1: Time-averaged results. *Journal of turbomachinery*, *131*(132), 021003. https://doi.org/doi.org/10.1115/1.2948968

Tan, M., He, N., Liu, H., Wu, X., & Ding, J. (2016). Experimental test on impeller clocking effect in a multistage centrifugal pump. *Advances in Mechanical Engineering*, *8*(4), 1687814016644376. https://doi.org/10.1177/1687814016644376

Tan, M., Lian, Y., Wu, X., & Liu, H. (2019). Numerical investigationof clocking effect of impellerson a multistage pump. *Engineering Computations*, *36*(5), 1469-1482. https://doi.org/10.1108/EC-09-2018-0413

Walker, G. J., & Oliver, A. (1972). The effect of interaction between wakes from blade rows in an axial flow compressor on the noise generated by blade

interaction. *Journal of Engineering for Gas Turbines & Power*, *94*(4), 241-248. https://doi.org/doi.org/10.1115/1.3445679

Wang, C. N., Yang, F. C., Nguyen, V. T. T., & Vo, N. T. (2022). CFD analysis and optimum design for a centrifugal pump using an effectively artificial intelligent algorithm. *Micromachines*, *13*(8), 1208. https://doi.org/doi.org/10.3390/mi13081208

Wang, W., Pei, J., Yuan, S., & Yin, T. (2018). Experimental investigation on clocking effect of vaned diffuser on performance characteristics and pressure pulsations in a centrifugal pump. *Experimental Thermal and Fluid Science*, *90*, 286-298. https://doi.org/doi.org/10.1016/j.expthermflusci.2017.09.022

Wei, J., Diyi, C., Wang, Y., & Ting, L. (2018). Experimental and numerical investigation on the influence of the clocking position on hydraulic performance of a centrifugal pump with guide vane. *Journal of Vibroengineering*, *20*(6), 2469-2485. https://doi.org/doi.org/10.21595/jve.2018.18758

Xiaoran, Z., Yexiang, X., Zhengwei, W., Hongying, L., Soo-Hwang, A., Yangyang, Y., & Honggang, F. (2018). Numerical analysis of non-axisymmetric flow characteristic for a pump-turbine impeller at pump off-design condition. *Renewable Energy*, *115*, 1075-1085. https://doi.org/doi.org/10.1016/j.renene.2017.06.088

Yang, B., Li, B., Chen, H., & Liu, Z. (2019). Entropy production analysis for the clocking effect between inducer and impeller in a high-speed centrifugal pump. *Proceedings of the Institution of Mechanical Engineers, Part C: Journal of Mechanical Engineering Science*, *233*(15), 5302-5315. https://doi.org/doi.org/https://doi.org/10.1177/0954406219843946

Zhang, X. Y., Jiang, C. X., Lv, S., Wang, X., Yu, T., Jian, J., Shuai, Z. J., & Li, W. Y. (2021). Clocking effect of outlet RGVs on hydrodynamic characteristics in a centrifugal pump with an inlet inducer by CFD method. *Engineering Applications of Computational Fluid Mechanics*, *15*(1), 222-235. https://doi.org/doi.org/10.1080/19942060.2021.1871961

Zhu, X., Xie, C., Jiang, W., & Li, G. (2023). Numerical investigation of clocking effect on irreversible energy loss in volute for centrifugal pump with vaned diffuser based on entropy generation method. *Proceedings of the Institution of Mechanical Engineers, Part C: Journal of Mechanical Engineering Science*, 09544062221148041. https://doi.org/doi.org/10.1177/09544062221148041